# A Comparison of Surface Deformation Measurement Methods for Slopes

Chung R. Song [1,*], Richard L. Wood [1], Binyam Bekele [2], Nikolas Glennie [3], Alex Silvey [3] and Mitra Nasimi [1]

[1] Department of Civil and Environmental Engineering, University of Nebraska-Lincoln, Lincoln, NE 68588, USA

[2] Ardaman and Associates, Inc., Affiliated to Tetra Tech Company, Orlando, FL 32809, USA

[3] Nebraska Department of Transportation, Lincoln, NE 68502, USA

* Correspondence: csong8@unl.edu

**Abstract:** This study aimed to promote an efficient and reliable collection of deformation data for earthen slopes by comparing the Total Station (TS), Distributed Strain Sensing (DSS), and Uncrewed Aerial System (UAS)-based deformation measurement methods. The TS-based method was a two-person task with a longstanding "tried and true" reputation, and it provided acceptable results. However, it included a major portion of manual work in the field, potentially consuming extended time to obtain high-resolution data. The DSS-based method was a fiber optic cable-based one-person work, and it showed substantially faster and easier measurement. This method possessed the capability of collecting unattended measurements. The method also required anchor posts to measure deformation in segmented sections; some anchor posts became loose from shrinkage cracks and resulted in invalid measurements, particularly for soils of high plasticity. The UAS-based method was an aerial photogrammetric method. It provided an extremely high-resolution deformation profile but required a manual survey for an elevation check at reference points, although the surveying took a short amount of time by utilizing a Global Navigational Satellite Survey (GNSS) technique. This method required one operator and an assistant. From a comparison of the characteristics of the three different methods, it was found that each technique has its pros and cons, and the combination of different methods may greatly enhance the accuracy and convenience of the measurement.

**Keywords:** slope monitoring; fiber optic DSS (Distributed Strain Sensing); UAS (Uncrewed Aerial System); deformation

## 1. Introduction

Civil infrastructure is built to enhance the quality of life of the general public. Slopes are a part of these civil infrastructure systems, typically designed and constructed based on sound science and engineering knowledge. These slopes, however, occasionally fail, causing life losses, structural damage, and accessibility issues (e.g., road closure and detour). One of the methods that may fill the gap between practice and science and minimize the occurrence of slope failures may be field monitoring. By analyzing the behavior of the critical slopes based on accurate sensor data, engineers may be able to foresee the possibility of failure before a failure occurs. With well-developed modern sensors, these tasks are seemingly straightforward. However, it is noted that predicting the likelihood of failure is only reliable when the characteristics of different sensors and sensing systems are rationally evaluated.

Many new types of sensors and sensing systems have emerged in recent years and decades. Some of them may have a high potential to be excellent sensor and sensor systems for health monitoring at a much lower cost than others. A large amount of detailed sensor information for traditional sensors is found in the literature, such as Dunicliff [1] and Hanna [2]. The information on newer sensors, such as fiber optic cable-based Distributed

Strain Sensors (DSS) or Distributed Temperature Sensing (DTS), are addressed by Soga et al. [3] and Gupta [4]. In addition, an Uncrewed Aerial System (UAS)-based deformation measurement system is also used to survey the deformation of a large area, as addressed by Adamopoulos and Rinaudo [5], Seier et al. [6], and Cook [7]. The use of GPS itself as a stand-alone deformation sensor is also reported (Zhang et al. [8,9]). However, the successful application of sensors in general may substantially depend on the proper understanding/evaluation of the characteristics of the sensors and sensor system as addressed by Song [10–12]. Particularly for these new kinds of sensors such as DSS, DTS, and UAS, all steps in field instrumentation—sensor selection, installation, data taking, and data analysis—should be carefully evaluated and cross compared. However, cross-comparisons of these new sensors hardly exist presently.

This study evaluates the features and field applicability of these newer measurement systems based on experience in measuring the deformation for two roadside slopes. The two sites have varying conditions, such as soil type, geographical location, and weather condition. In addition, this study included the traditional Total Station (TS)-based measurement result in the comparison, even though its usage was limited to only the first site. Findings from the field instrumentations and performance data from these sites, therefore, will benefit the geotechnical instrumentation community as a whole.

## 2. Principles of New Measurement Methods

### 2.1. DSS-Based Deformation Measurement

The DSS-based measurement system is a modern method to sense the deformation of civil infrastructures. The technique is a derivative of time domain reflectometry (TDR), which is widely used in the telecommunication industry to detect the location of a troubled/damaged point in a telecommunication cable. The TDR identifies the existence of the trouble/damaged points, because the existence of the reflected wave indicates the existence of a partial or complete discontinuity in the cable, as shown in Figure 1.
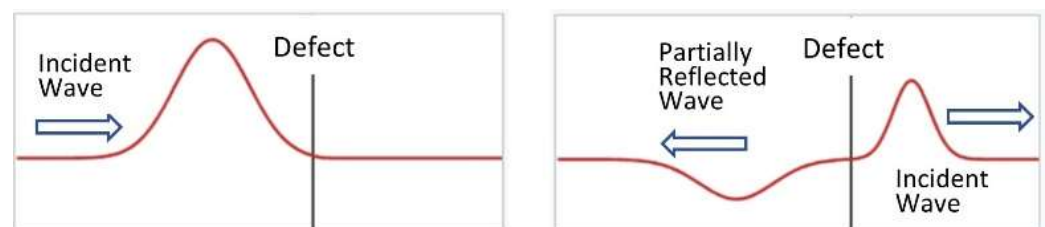
**Figure 1.** Time domain reflectometry (TDR) (Revised plot based on Oleg [13]).

When the technique is used with the travel time (distance) ranging method, it can locate the position of the defect (distance from the measurer). Then, the technique essentially serves the role of a radar. When the technique is applied to optical laser light and fiber optic cable, it is called optical time domain reflectometry (OTDR). Fiber optic cables have additional characteristics such as Brillouin scatter and Ramen scatter. Brillouin scatter is the scatter of laser light created by the strain caused in the cable, while the Ramen scatter is the scatter of laser light created by the temperature anomaly caused in the cable. Therefore, combining radar-like distance ranging capability, strain detecting capability, and temperature detecting capability, the DSS system can be used for monitoring the deformation and temperature in structures with a high spatial resolution.

Typically, the frequency shift due to Brillouin scatter is in the 9 to 11 GHz range, while that, due to the Raman scatter, is higher, reaching typically up to the 13 GHz range (Zou [14]). Therefore, it seems that the deformation and temperature may be obtained without mutual interference. However, the DSS system is not faultless, as addressed below. It is noted that the temperature fluctuation may cause thermal strain in the cable and cause the additional Brillouin frequency shift. Lu et al. [15] reported the effect to be approximately 2.03 $\mu\varepsilon/°C$ temperature-driven strain shift or 1.03 MHz/°C frequency

shift for $SiO_2$ core. However, this magnitude can be slightly different depending on the properties and thickness of core and cladding materials, as reported by Beugnot et al. [16] and Toshio et al. [17]. Therefore, it is logical to presume that a low-level strain (10 to 20 $\mu\varepsilon$) measured from OTDR may not always indicate the mechanical deformation or strain of a target structures. It could be just the result of the temperature fluctuation. In addition, the strain-dependent Brillion frequency shift is not just by the axial strain. It can be affected by the shear or twisting strains (Kazi et al. [18]) because it is affected by any mechanism causing changes in the lattice structure of a material (Zel'dovich et al. [19]). Therefore, a careless handling (e.g., unwinding) of the fiber optic cable (without utilizing an unwinding roller) may cause an additional frequency shift, requiring attention from the installers/operators until quantitative research clarifies the twisting effect.

To further facilitate the separation of mechanical strain and thermal strain, a cable with tight buffered wire and loose tubed wire, as shown in Figure 2. This cable system is also used to obtain the mechanical strain by subtracting the thermal strain in the strain relief loose tube cable from the mechanical + thermal strain in the tight buffered cable. However, accurate separation of mechanical strain and thermal strain is still a challenging task, as the cable in the loose tube has a vinyl or polymer jacket that may interfere with the thermal stain in the fiber optic cable. Therefore, further research is needed to accurately separate these two different strains. Further details of the OTDR-based DSS system are found in a study by Parker et al. [20].
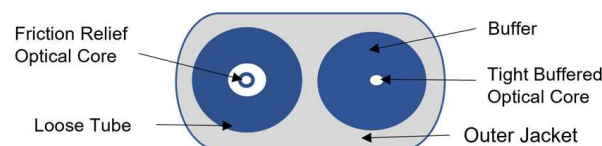
**Figure 2.** Cross section of fiber optic cable for physical strain and temperature measurement.

The equipment used in this study is the LIOS Pre.Vent system, which takes readings in 25 cm intervals, computes the average of four numbers, and provides average strain and temperature for every 100 cm intervals. The workflow was simple: connect the LIOS device to the fiber optic cable, turn on measurement software, and wait until the device finishes the data collection procedure. Then, compare the strains computed at each point with the initial readings and find the difference that is the deformation between two different measurement times. In this study, the strain caused by the movement(deformation) of the structure is monitored by tight-buffered cables, as shown in Figure 2, while the temperature is monitored by strain relief loose tube cables. Therefore, this study partially nullifies the so-called strain-temperature coupled effect to a certain degree.

### 2.2. UAS-Based Deformation Measurement

UAS-based surveying is an efficient way to collect data even from very large areas. In recent years, UAS-based surveying has become one of the popular methods due to its low cost, efficiency, and accuracy. In some cases, it is the only method to collect data when an area is remote or hard to reach. This method can provide terrain information in the form of a point cloud or an orthomosaic image. Several researchers have used this technique to monitor and measure the changes in multiple different cases. Deligiannakis et al. [21] utilized UAS for post-fire surveying to detect the areas of sliding potential. In addition, multiple researchers, Mahalingam et al. [22], Watts et al. [23], and Mozas-Calvache [24], have utilized an UAS-based method to generate the digital topographic map, collect the deformation data, and analyze the potential for slope failure. In this research, UAS surveying is used to monitor the potential movement of slopes, with a focus on surface deformation measurements only.

The technique needs to have ground reference points visible to a UAS. Then, a UAS flies through the target area with a camera that takes high-resolution images with a dedicated GNSS receiver (Global Navigation Satellite System) to enable the PPK (Post-

Processing Kinematic) technique to obtain centimeter-level positioning. The required base station should be set up to correct the GNSS data of the drone; in this study, the UAS platform was WingtraOne. After the flights, aerial images, UAS-based Rinex file, the estimated base station position were obtained from OPUS (Online Positioning User Service), and the base station Rinex file was needed to process together to add the geographic information to imagery data at the centimeter level. At the end of this procedure, a 3D point cloud of the surveyed area was developed, as shown in Figure 3 as an example. The grainy image in the figure is due to the discrete nature of the data in the point cloud, highlighting the extremely high-resolution points that represent the digitized scene (containing the 3D coordinate information at the centimeter level typically).
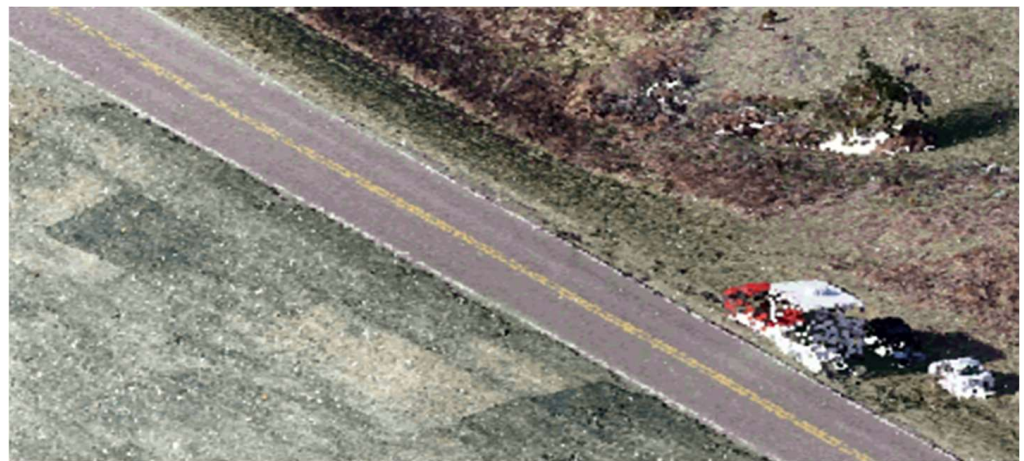
**Figure 3.** Example view of a point cloud as collected from a UAS platform.

The combined data set makes it possible to conduct a comparison of the coordinates of point clouds from multiple different times. This will allow one to compute the spatial differences through a technique called change detection. Once fully processed, the point cloud data set was extremely dense due to the high-resolution cameras flown in modern-day UAS platforms flying at above-ground altitudes that are close to the ground. The actual overview of point clouds and derived deformation profiles are shown and discussed in the following sections.

## 3. Project Sites

Nebraska has distinct surface soil conditions due to its unique geological history. A simplified geological history of this area, based on Ford [25], is summarized as follows. North, West, and mid-Nebraska were under the old "Western Interior Sea (also called Niobrara Sea)" 145 to 66 million years ago. Deposits during this time primarily formed marine shales with layers of chalks and sandstones at the top, as shown in Figure 4a. Then, the current Rocky Mountains area rose above the sea level during the late Cretaceous and early Tertiary periods, and drained water from the Western Interior Sea, converting the area to a dry prairie. Subsequently, this area received water from the Rocky Mountains, accumulated thick fluvial deposits of non-cohesive materials, stored water in the fluvial deposits, and formed a gigantic underground water reservoir called the Ogallala Aquifer. The flowing water also washed out parts of the marine shales and chalks, creating occasional deposits of marine-sourced expansive clays in the area where the Niobrara and Missouri Rivers flow today. Therefore, slope failures in northern Nebraska where one of the study areas is located are believed to be related to these slick and expansive clay deposits.
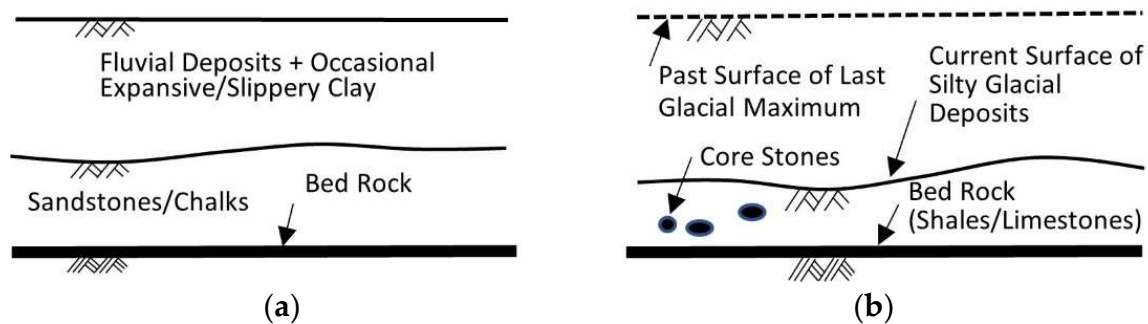
**Figure 4.** Schematic Layer Profiles in Nebraska (Note: Figures are not in scale). (**a**) Typical soil profile in North, West and Mid-Nebraska. (**b**) Typical soil profile in East Nebraska.

On the other hand, East Nebraska, where another study location is located, had shales and limestone as bedrock which appeared above the sea level from the Cretaceous period. Then, this area was covered by the Last Glacial Maximum (LGM) about 19–26.6 k years ago, and it formed the thick (up to 50 m) glacial deposits of young silty soils and occasional core stones as surface soils, as shown in Figure 4b, after the glacier melted away. Many slope failures in eastern Nebraska are believed to be related to the strength reduction of this silty deposit (Song et al. [26], Eversol [27]).

Engineers applied retrofitting techniques to failed slopes in these areas with dedicated monitoring systems, as these slopes failed several times. Furthermore, the engineers gained knowledge of the comparative performance of different monitoring systems, particularly the new deformation monitoring systems. This paper provides a constructive comparison of a different deformation measurement system based on the experience in slopes in two different locations: one for the glacial till site (I-180 in Lincoln) and another for the slippery marine deposit site (Highway-84 in Verdigre).

### 3.1. Interstate-180 (Lincoln) Site

I-180 is one of the interstate highway systems connecting the downtown of Lincoln, Nebraska to I-80, one of the East-West bound major highways traversing from San Francisco to New York. The slope is 9 m high and 27 m wide (1V:3H) with a history of previous slidings and repairs, as reported in studies by Bekele et al. [28] and Song et al. [29]. The soil profile for this slope consists of mostly glacial tills with loamy silts, as shown in Figure 4b. However, it is noted that the loamy silts in this site are not volcanic loam; they are layers of fine glacial till particles blown by winds and sedimented.

The slope movement occurred, as shown in Figure 5a, and the crack progression was monitored with PVC surface posts and a fiber optic cable-based DSS system, as shown in Figure 5b, to quantify the rate of the movement and design a countermeasure. The DSS system consisted of 15 cm diameter PVC pipe posts and a fiber optic cable with tight buffered optical fiber for strain measurement, and a loose tube type fiber optic cable for temperature measurement, as shown in Figure 2. The fiber optic cable was arranged in three rows of four posts, and a total of 12 points were installed to cover the whole slope, as shown in Figure 6. The cable was wrapped twice around each post under tension and secured with tape to minimize slippage. Tension was applied to the cable between each post so that the cable would not slack, and it was expected that the relative movement of the posts would change the applied tension and associated deformation on the cable, enabling the DSS to measure it.

(**a**)             (**b**)
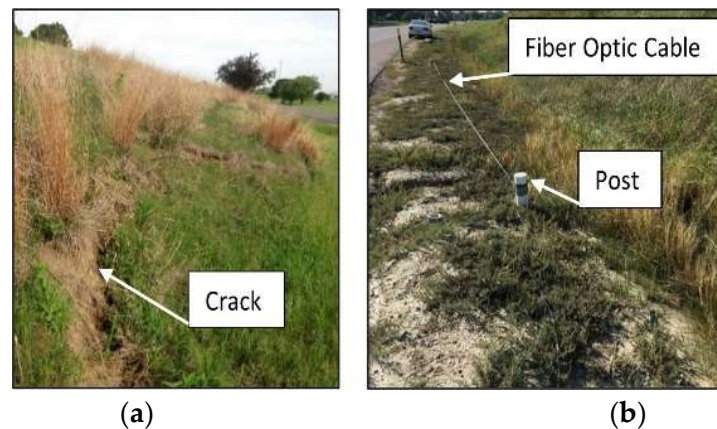
**Figure 5.** Scene of I-180 Slope. (**a**) Crack on I-180 Slope. (**b**) DSS System Installed on I-180 Slope.
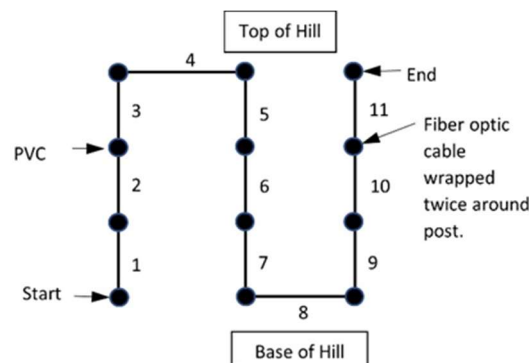
**Figure 6.** Arrangement of DSS Cable and Posts.

In addition to the DSS-based measurement, UAS-based surveying was conducted as a separate system to monitor the deformation of the slope. UAS expected to measure the deformation throughout the entire slope and not just at discrete locations such as the DSS and surveying posts. Anchor posts for the DSS system shown in Figure 5b were used as reference points to enhance the accuracy of the UAS surveying result. The UAS system collected a sequence of photos that can be used for the 3-D reconstruction of the slope geometry using Pix4DMapper. For this site, the work was accomplished using a dedicated UAS, a DJI Mavic Pro 2 UAS platform with an onboard 20.8 MP camera. At the same time, multiple marker points were added to the target surveying area before acquiring the aerial imagery. The marker points were placed on locations that can be observed in aerial imagery, then a GNSS-enabled rover was used to record their coordinates. These points are important for surveying since their true coordinates are known; consequently, they should provide an accurate position in images of the dataset. After surveying, imagery data and coordinates of the marker points were imported into Pix4DMapper. In the next step, the surveyed points were divided into CPs (CheckPoints) and GCPs (Ground Control Points). GCPs are selected in a few images to revise image coordinates and match them with the real-world coordinates at the centimeter level accuracy. CPs are used as additional points with real-world coordinate information to confirm the model's accuracy at the centimeter level. Using GCPs significantly increases the accuracy of the surveying, as the GPCs enable restraints on the model to limit the errors.

### 3.2. Highway 84 (Verdigre) Site

Highway 84 is a Nebraska state route connecting the town of Verdigre, Nebraska to Bloomfield, Nebraska. The soil condition is primarily fluvial deposits transported from the Rocky Mountains as shown in Figure 4a. However, the nearby Niobrara and Missouri Rivers, located about 10 to 20 km away from this site, washed out and spread the underlain

marine sourced shales (Pierre Shale), which contained expansive clay minerals. It is also noted that the layers of chalk, the source of slippery layers, are easily found along the cliffs of the nearby Missouri river. Classification of clayey soils in this site was classified as CH to CL (the borderline of highly compressible clay and low compressible clay). These soils are called "Blue Clay" by local residents, which are in fact a mixture of loosely packed Pierre shales and dark clayey soils. This area is a region of Nebraska that is well-known for various slow landslides caused by the unique soil characteristics and topography.

Minor cracks appeared on the shoulder of Highway 84 in the summer of 2018 (Song et al., [29]), as shown in Figure 7, and they developed to noticeably wider ones afterward. Consequently, the Nebraska Department of Transportation (NDOT) decided to remove the crack-infested field soils from the affected area and rebuild the slope, as shown in Figure 8a, with off-site borrow soils, which do not include expansive clay minerals. The brought-in soils have the classification symbol CL with fine content of 30%. In addition, Xanthan (a biopolymer)-based stabilized soils were applied at the bottom of the slope. The similar DSS system and PVC pipe anchors as the ones used for the I-180 site were installed along the slope, as shown in Figure 8b, inspired by the promising results and experience with the I-180 slope. Additionally, it was noted that the same crew conducted the UAS-based topography survey with a set of upgraded UAS equipment as follows.
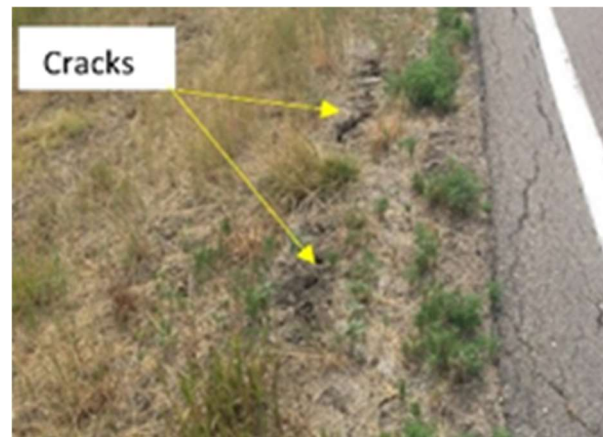
**Figure 7.** Initial Cracks Appeared on Highway 84.
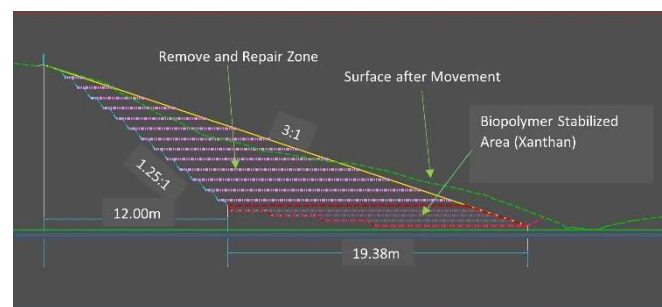
**Figure 8.** Cross Section and Pictue of Verdigre Slope. (**a**) Retrofitting design of the slope. (**b**) Anchors for DSS and UAS reference points.

                                                                                                                

The UAS system for this site collected a sequence of high-resolution imagery data that might be used for the 3-D reconstruction of the slope geometry, using a Pix4DMapper. This was accomplished through the use of a dedicated surveying UAS, a WingtraOne fixed-wing UAS platform with an onboard Sony 42 MP camera, and a built-in multi-frequency PPK (Post-Processing Kinematic) GNSS antenna of the UAS. The imagery data collected with this UAS were accurate enough without ground control, as this had been confirmed by the research team and others (e.g., Chudley et al., [30]). To achieve this accuracy without the use of GCPs, data were collected using the PPK technique, with one GNSS receiver on the UAS and the other being the static base station. The base station was logged continuously throughout the UAS flight, and the location of the base station was obtained using OPUS (Online Position User Service). Here, OPUS provided an accurate estimate of the base station, specifically for International Terrestrial.

Reference Frame coordinates of 0.6 cm horizontally and 2.5 cm vertically. Due to the known accuracy of the PPK platform and the wet slope in the field, CPs were not deployed nor deemed necessary. For likewise reasons of wet and slippery slopes, the TS-based surveying technique was also not deployed for safety. The accuracy of the tagged pictures was 2 cm horizontally and 4 cm vertically, with the constructed point clouds having an average ground sampling distance of 1.04 cm.

## 4. Measurement and Results/Discussion

To conduct fiber optic sensing readings, the necessary components included a controller, a 120 V AC power supply, a sensing cable with spliced connectors, an ethernet cable, and a computer equipped with specialized software for the controller. The controller was connected to the 120 V AC power supply; this research utilized a large 1000 W lithium-ion battery for I-180 slope, and a 2000 W pure sine wave generator for Highway 84 slope to provide power in the field. The connector ends were examined for obstructions using a fiber scope and cleaned with alcohol wipes, if necessary, before being connected to the controller. It was imperative that each connector be placed into the same port for each reading because the calibration of each strand of cable was individualized. An ethernet cable was used to connect the controller to a computer. Once plugged into the controller, an IPV4 connection between the controller and the computer was established for the devices to share information. The computer software for the controller (Charon 4) was finally utilized to calibrate the device to each cable strand, take readings, and manipulate data.

### 4.1. I-180 Slope

One of the results depicted in Figure 9a illustrates the overall deformation measured by the DSS, situated just below the crack location in Figure 5a. This measurement accounts for the average strain multiplied by the length between anchor poles. Notably, this output indicated substantial movement at the toe of the slope that was imperceptible to the naked eye. Subsequently, during field reconnaissance on 26 April 2019, a pot-belly-like deformation was observed in segments 6 through 10, which qualitatively confirmed the findings presented in Figure 9a. This measurement result is notable considering that the slope was actually visually identified to have failed in May 2019.

It is worth mentioning that the measurement between 9 November 2018, and 17 January 2019 could not be obtained due to unstable readings from the device. Although the exact cause was not determined, the research team speculated that the extremely cold temperature during that period may have contributed to the issue. Moreover, it was observed that the fully charged lithium-ion battery showed 12.7 V in the laboratory exhibited less than 11 V while in the field. While a drop in voltage of this magnitude is typical for lithium-ion batteries in cold weather, it may affect the performance of sensitive equipment. The measurement readings resumed on 17 January 2019 and persisted until 25 April 2019. However, in May 2019, the slope experienced significant movement, and the measurement readings were discontinued.

(**a**)

(**b**)

(**c**)
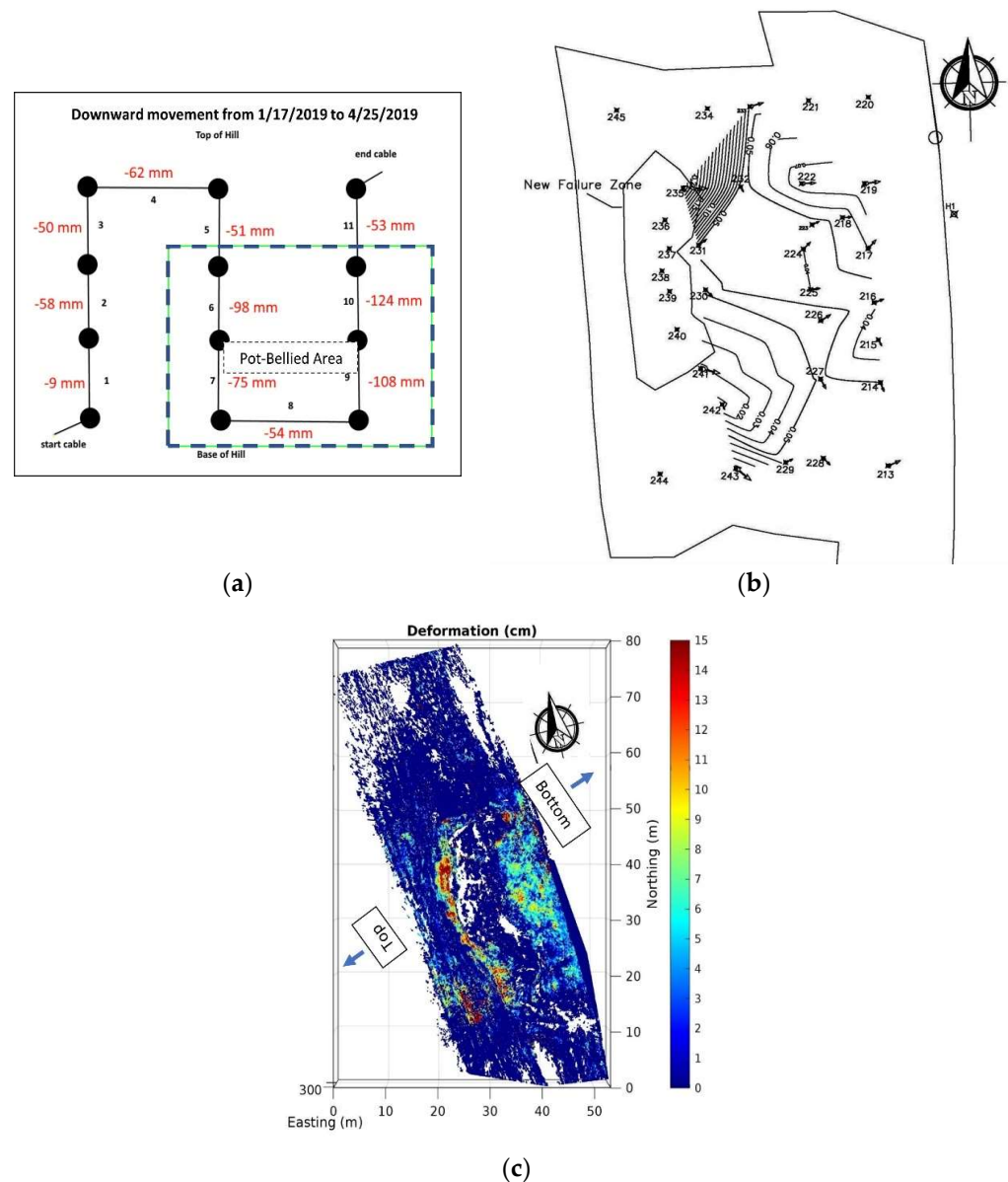
**Figure 9.** Deformation profiles of I-180 slope obtained from different methods. (**a**) Downward deformation monitored by DSS. Note: (100 mm = 2.5% downward strain) (**b**) Deformation (m) contour measured by TS (Difference between before and after the failure. Arrows indicate the direction of the movement). (**c**) Deformation profile from the UAS-based method (Unit of the color bar is in cm).

For the TS-based results, the vector square root sum was applied to the deformation (in three dimensions) obtained from the total-station-based surface survey, shown in Figure 9b as a two-dimensional plot. The magnitude of deformation shown in Figure 9b includes the deformation that occurred from the failure in May 2019. The figure shows a sharper deformation gradient towards the north, where a substantial vertical drop and opening were observed. At the downslope side, the deformation is approximately 7 cm, which is lower than that measured by the DSS. However, it is noted that DSS-measured deformation is the relative deformation between anchor poles, not the total deformation. It is also noted that the DSS-measured deformation data may be affected by the temperature, especially during extremely cold weather. Therefore, in this study, DSS data were not corrected for the temperature, nor edited to show the total deformation, due to the lack of science/engineering for clearly separating the effect of temperature from DSS-measured

deformation installed between semi-rigid anchors. Therefore, a direct comparison of the deformation magnitude of the survey and that of DSS was not conducted.

UAS-based deformation surveying is based on the multiscale cloud comparison (M3C2) algorithm within the CloudCompare software, as developed by Lague et al. [31]. This algorithm finds differences between two-point clouds (at different time periods) by calculating the average distance of matching points. This algorithm is point cloud-based; therefore, it has fewer geometry-related errors. Because of this feature, the M3C2 method has gained popularity in recent years, as addressed in DiFrancesco et al. [32] and Bolhasan et al. [33]. In this study, the point clouds of the site are compared against each other from Spring 2019 to Spring 2021.

A UAS-based method in Figure 9c shows concentrated deformation along the failure line (shown in bright green). Some areas are impeded due to the presence of heavy vegetation and no data appear in these regions (white spots). The intermittent red spots (at the top failure line and the bottom) indicate localized but particularly high deformation areas. The survey is based on two results, one before the failure and another after the failure. The general trend of deformation in the UAS-based method aligns with the TS-survey outcomes. However, the magnitude of deformation is comparatively higher in the UAS-based approach when compared to the TS survey, but it is in line with DSS results showing similar pot-bellied deformation at the downstream side (the zone with light blue color). This disparity between TS and UAS method could be attributed to differences in measurement principles and dates employed for the TS survey and DSS. Notably, weather conditions (i.e., temperature, rain, and wind) were crucial factors for DSS, TS, and UAS-based measurements.

To summarize the findings of the deformation measurement techniques, it is challenging to determine which method is superior for this particular site. In light of the possible deformation profile of the slope after failure, ranging from sub 10 cm to almost 1 m, as demonstrated by Bekele et al. [28], all three techniques possess an inclusive sensitivity in the mm range, and indicate the location of the failure zone accurately. Therefore, a detailed error analysis was unnecessary. However, there are differences in measurement convenience that can be noted, as described below.

The DSS was easy to install in the field and take measurement readings. The fiber optic cable was easy to purchase and the price was reasonable enough to be easily acquired, particularly when considering the number of data points one could obtain. The measuring method was based on valid Optical Physics; however, Brillouin scatter and Raman scatter might be coupled in cases when the temperature fluctuation was high, then the coupling of the mechanical strain and the thermal strain might have an unignorable effect on the measured deformation. Currently, it is not possible for practicing engineers to distinctly differentiate between mechanical strain and thermal strain. Notably, the DSS method has a distinct characteristic of measuring the relative deformation between anchor points, rather than the absolute deformation measured in TS and UAS-based measurements. To measure absolute deformation, reference anchor points located outside of the deformation zone may need to be installed so that the relative deformation could be calibrated to the total deformation.

DSS fiber optic cables required more delicate handling than traditional copper cables. Their appearance was similar to that of typical electrical cables. Inexperienced users tended to handle them like a copper cable and ended up with a damaged cable, failing to provide any data or reliable data. Splicing the fiber optic cable was not easy in the field, particularly when environmental factors such as cold weather and dusty conditions were taken into consideration. A fiber scope, a professional-grade splicer, and a DSS interrogator (readout unit) were often used to inspect the damage in the fiber, but they might be cumbersome to use or expensive, prohibiting wide applications. After overcoming these difficulties, DSS needed about one hour to complete a set of measurements, which was the quickest method among the three techniques. A trivial but additional benefit is that the technique needed only one operator. In addition, the DSS technique may be set to self-monitoring mode, and

able to take the measurement and transmit the data wirelessly regardless of the weather condition, even after the ground was covered by deep snow.

Surveying is a conventional method and was supposed to be an easy technique. However, the accuracy of the result may heavily depend on the skill and experience of the surveyors. This technique required two persons, and it took a longer amount of time compared to DSS and UAS-based techniques. In addition, this technique might not be an ideal fit for rugged terrains. However, with experienced surveyors, this technique is a time-proven technique and may economically overcome difficult environmental factors (except thick snow covering), which may pose challenges to other techniques discussed.

The UAS-based technique used to be an expensive technique, and it had been used only in limited applications. With the availability of UAS systems at an affordable price, and with enhanced camera quality, this method has become a convenient option. The technique provides an unmatched high-resolution data set compared to both the TS and the DSS methods. UAS seemed particularly advantageous for applications on wide and rugged terrains. Although, this technique required two skilled crew members, including an operator with a UAS pilot's license and an assistant to monitor highway safety. UAS also resorted to dedicated software to compile and analyze an extremely large data set, which might be expensive and time-consuming depending on the system being used. It was, however, noted that the data reduction time for UAS based technique was not noticeably longer than other techniques.

Although cross-comparison of errors for the three techniques was contemplated, it was ultimately not executed due to the significant differences in measurement principles, as previously mentioned. As previously noted, the DSS was intended to measure relative movement rather than changes in coordinates, while UAS and TS provide total deformation. Nonetheless, all three methods effectively indicated the location of the failure zone.

*4.2. Highway 84 Slope*

Figure 10a displays the layout of the overall deformation measurement line utilizing the DSS method. Meanwhile, Figure 10b depicts the DSS based strain measurement results, with negligibly low strain. Here, the DSS cables were tightly wound around the posts three times, resulting in additional bending strain in the DSS cables. Notably, the ambient temperature at the site was frequently below the freezing point. Based on previous experience—the 1000 W lithium-ion battery did not work very well for the I-180 site on cold days—a 2000 W pure sine wave generator was used for this site.

The overall strain was at the ±50 micro strain level. Assuming that the thermal strain might take about 20 microstrains, as previously discussed for the case of the I-180 slope, the mechanical strain was ±30 micro strain range, which is practically an elastic strain level in clay-reach soils. This analysis is based on the notion that the behavior of clayey soils is essentially elastic when the strain level is close to or lower than 50 microstrains (Song and Stokoe II, [34]). The measurement readings of this site were halted due to snow. In Spring 2021, measurement readings were resumed, but the DSS cables were observed to be loose in many sections. Careful investigation showed abundant animal droppings in the measurement site. According to a local resident, the issue with the DSS cables could be attributed to the activity of wild deer in the area. As a result, the cables were re-tightened and measurement readings resumed in the summer of 2021. However, it was discovered that the cable posts had become loose again due to the widespread shrinkage cracks found around them. Unfortunately, the DSS cables installed at the Highway 84 slope failed to provide the expected data. Moreover, it is noted that the DSS monitoring system has a potential limitation in that the obtained signals may not be as distinct as those obtained through the FBG (Fiber Bragg Grating) method, which utilizes factory-generated clear cracks or mirrors (Kretsch et al., [35]), despite being a more cost-effective alternative. Additionally, it is important to handle the DSS cables properly as slight mishandling can result in damage and prevent the glass fiber from transmitting accurate signals. Therefore, proper knowledge and handling of the fiber optic cable are critical for the successful

deployment of the DSS monitoring system. However, the economy of the DSS method is not matched by the FBG method because the technique essentially utilizes the same fiber optic cable used for the telecommunication business.
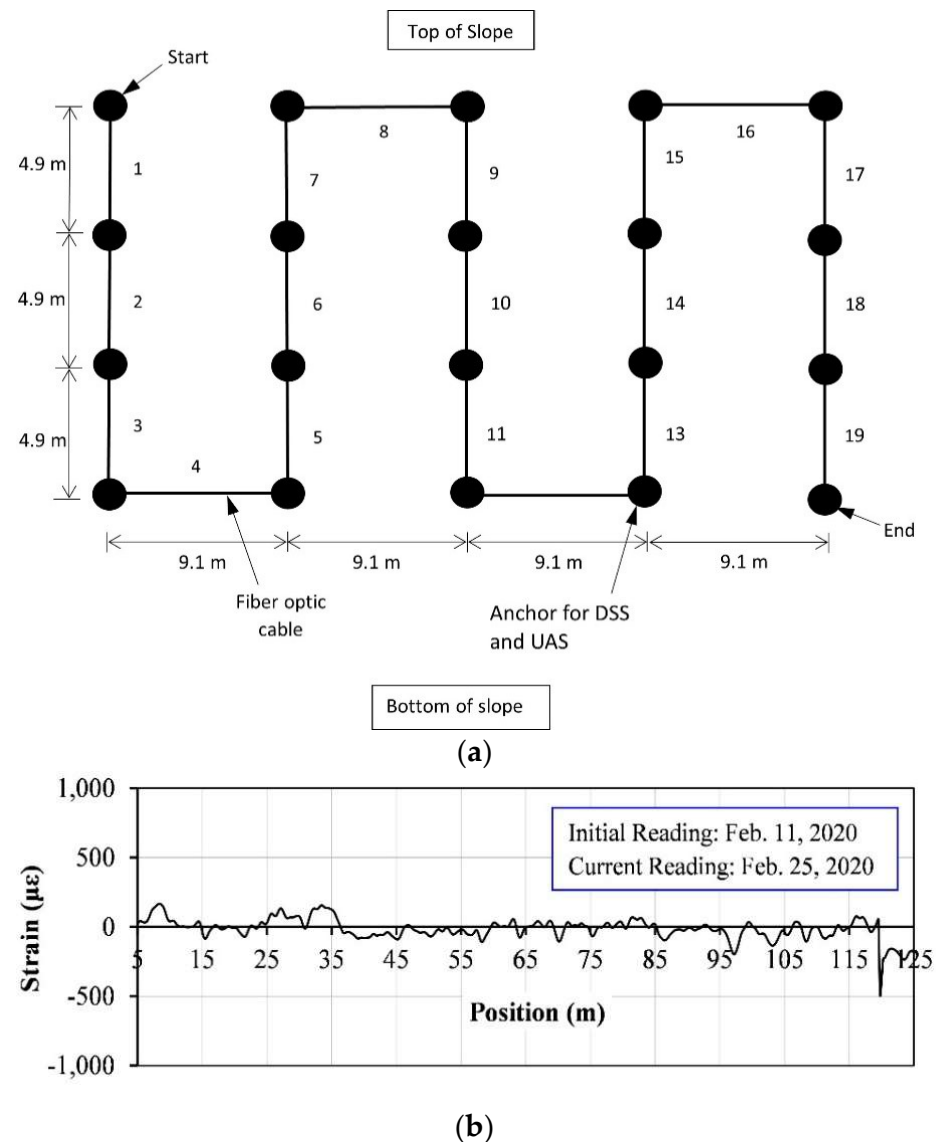
**Figure 10.** Instrumentation on Highway 84 slope. (**a**) Alignment of DSS line (Large solid circle: PVC Pole, Black Line: DSS line). (**b**) Measured Strain by DSS.

On the other hand, the UAS-based method showed a clear deformation profile of the slope and surrounding area, as shown in Figure 11. The target area is shown in the black inset box. Due to the upgraded hardware, the resolution of the deformation is higher than in the previous case for the I-180 slope. The red color shown at the bottom indicates approximately 15 cm of false settlement caused due to the disturbance and surface movement by the mobilization of the drilling equipment.

Overall, the slope showed zero (blue to green color) to 8 cm (red color) deformation, but it did not indicate any major movement of the slope.
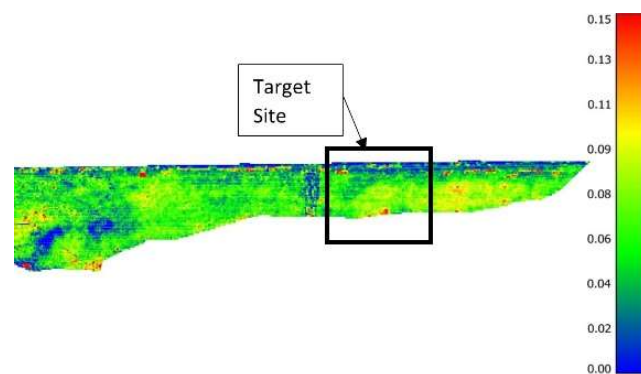
**Figure 11.** UAS-based deformation profile of Highway 84 (From Spring 2019 to Spring 2021, Unit of the color bar is in m).

## 5. Conclusions

This study evaluated the features and field applicability of different deformation measurement methods—Distributed Strain Sensing (DSS), Uncrewed Aerial System (UAS), and Total Station (TS)—based on multiple years of experience in monitoring deformation for two roadside slopes. The two sites have varying conditions such as soil type, geographical locations, and weather conditions. From the comparative study, the following conclusions are obtained.

The DSS-based method was the quickest and easy method to measure the deformation of the ground surface. The installation of measurement poles was easy. The measurement took typically an hour for one site and needed only one operator. The method was little impaired by vegetation or snow covering once the system was installed. Training an operator was easy. The remote control and remote measurement were possible in some models.

However, the fiber optic cable of DSS might suffer from the activity of wild animals and low-temperature-related voltage drops from the batteries. In addition, the PVC posts driven into the ground were observed to be unstable due to shrinkage cracks which impaired measurement in highly plastic soils. Galvanized zinc pipes with a depth deeper than the frost depth and dry cracks might be more adequate for these soils. DSS used one long fiber optic cable; therefore, a damaged section anywhere in the system could disable the measurement after the damage point. To prevent this issue, installing redundant lines of DSS might be required.

The UAS-based method offered fast surveying even for a large job site. It was flexible to various weather conditions, except for snow coverings encountered in this study and some strong wind. The method could measure the 3-D surface deformation for the entire area of interest (not just at discrete points) with unmatched high resolution, providing deformation images extensively and clearly. The result of the UAS-based method generally agreed well qualitatively with those of other methods. The method provided rational deformation data even for relatively thick (0.3 m) vegetation areas.

Acquiring and maintaining the dedicated equipment, such as a high-quality UAS, UAS license, and specialized software, for the UAS-based method may be expensive. Moreover, it is recommended to have one drone operator and one highway safety crew member.

Traditional TS surveying was a popular technique; however, this method can be challenging to reliably deploy on certain slopes given moisture and safety concerns. The method was a two-person task; however, the output and measurement effectiveness were not better than the DSS or UAS-based methods. It was, however, noted that the TS method could be the most economic for certain slopes, particularly when the number of measurement points are not very high.

Due to the substantial differences in the measurement principles of the DSS, UAS, and TS, it was not possible to compare their errors directly. Nevertheless, these techniques are selectively preferred for their ability to remotely sense deformation, which is crucial for safety and operational purposes.

The authors propose a potential for combining different techniques to improve monitoring capabilities. While UAS can quickly monitor large and remote sites, it may face limitations in adverse weather conditions such as snow and strong wind. DSS can complement UAS by enabling remote/real-time measurements that can be conducted in small intervals and capture direct quasi-subsurface movement through anchor poles, indicating soil movement not affected by weathering elements.

**Author Contributions:** Conceptualization, C.R.S.; Methodology, C.R.S., R.L.W., N.G. and A.S.; Formal analysis, R.L.W.; Investigation, B.B.; Data curation, B.B. and N.G.; Writing—original draft, C.R.S.; Writing—review & editing, R.L.W., B.B., N.G. and M.N.; Supervision, A.S.; Funding acquisition, C.R.S. and R.L.W. All authors have read and agreed to the published version of the manuscript.

**Funding:** Authors of this research would like to acknowledge the funding from Nebraska Department of Transportation (SPR-P1(20)M110 and SPR-P1(17)M061). In addition, authors would like to appreciate Mr. Basil Abualshar for supporting field work.

**Informed Consent Statement:** Not applicable.

**Data Availability Statement:** The data is contained within this article.

**Conflicts of Interest:** The authors declare no conflict of interest.

## References

1. Dunnicliff, J. *Geotechnical Instrumentation for Monitoring Field Performance*; John Wiley and Sons, Inc.: Hoboken, NJ, USA, 1988; 577p.
2. Hanna, T.H. *Field Intrumentation in Geotechnical Engineering*; Trans Tech Publications: Stafa-Zurich, Switzerland, 1985; 843p.
3. Soga, K.; Ewais, A.; Fern, J.; Park, J. Advances in geotechnical sensors and monitoring. In *Geotechnical Fundamentals for Addressing New World Challenges Springer Series in Geomechanics and Geoengineering*; Lu, N., Mitchell, J.K., Eds.; Springer International Publishing: Cham, Switzerland, 2019; pp. 29–65.
4. Gupta, B.D. *Fiber Optic Sensors—Principles and Applications*; New India Publishing Agency: New Delhi, India, 2006; 294p.
5. Adamopoulos, E.; Rinaudo, F. UAS-Based Archaeological Remore Sensing: Review, Meta-Analysis and State-of-the-Art. *Drones* **2020**, *4*, 46. [CrossRef]
6. Seier, G.; Sulzer, W.; Lindbichler, P.; Gspurning, J.; Hermann, S.; Konrad, H.M.; Irlinger, G.; Adelwöhrer, R. Contribution of UAS to the monitoring at the Lärchberg-Galgenwald landslide (Austria). *Int. J. Remote Sens.* **2018**, *39*, 5522–5549. [CrossRef]
7. Cook, K.L. An evaluation of the effectiveness of low-cost UAVs and structure from motion for geomorphic change detection. *Geomorphology* **2017**, *278*, 195–208. [CrossRef]
8. Zhang, W.; Li, H.; Tang, L.; Gu, X.; Wang, L.; Wang, L. Displacement prediction of Jiuxianping landslide using gated recurrent unit (GRU) networks. *Acta Geotech.* **2022**, *17*, 1367–1382. [CrossRef]
9. Zhang, W.; Tang, L.; Li, H.; Wang, L.; Cheng, L.; Zhou, T.; Chen, X. Probabilistic stability analysis of Bazimen landslide with monitored rainfall data and water level fluctuations in Three Gorges Reservoir, China. *Front. Struct. Civ. Eng.* **2020**, *14*, 1247–1261. [CrossRef]
10. Song, C.R. Fact and Fiction in Field Instrumentation (Part II: Settlement Measurement). In Proceedings of the KGS Spring '96 National Conference, Seoul, Republic of Korea, 23 March 1996; Volume 74, pp. 205–220.
11. Song, C.R. Fact and Fiction in Field Instrumentation (Part III: Pore Pressure Measurement). In Proceedings of the KGS Spring '96 National Conference, Seoul, Republic of Korea, 23 March 1996; Volume 73, pp. 221–234.
12. Song, C.R. Fact and Fiction in Field Instrumentation (Part 1: Horizontal Displacement Measurement). In Proceedings of the KGS Fall '95 National Conference, Seoul, Republic of Korea, 28 October 1995; pp. III.1–III.8.
13. Oleg, A. Partial Transmittane.gif. 2007. Available online: https://commons.wikimedia.org/wiki/File:Partial_transmittance.gif (accessed on 30 October 2022).
14. Zou, W.; Ong, X.; Chen, J. Brillouin Scattering in Optical Fibers and Its Application to Distributed Sensors. In *Advances in Optical Fiber Technology*; InTech Open: Rijeka, Croatia, 2015. [CrossRef]
15. Lu, Y.; Li, C.; Zhang, X.; Yam, S. Determination of thermal residual strain in cabled optical fiber with high spatial resolution by Brillouin optical time-domain reflectometry. *Opt. Lasers Eng.* **2011**, *49*, 1111–1117. [CrossRef]
16. Beugnot, J.C.; Jeannin, C.; Tchahame, J.C.; Godet, A.; Ndao, A.; Sylvestre, T.; Ahmad, R.; Rochette, M. Temperature and strain dependence of Brillouin scattering in chalcogenide optical microwires. In Proceedings of the 1st International Conference on Optics, Photonics & Materials, Nice, France, 26–28 October 2016.
17. Toshio, K.; Tsuneo, H.; Mitsuhiro, T. Thermal effects on the Brillouin frequency shift in jacketed optical fibers. *Appl. Opt.* **1990**, *29*, 2219–2222.
18. Kazi, A.; Raja, A.; David, D. Suppression of Stimulated Brillouin Scattering using Off-Axis Twisted Core Fiber. In *OSA Technical Digest*; Paper SM3K.6; Optica Publishing Group: Washington, DC, USA, 2018.

19.    Zel'dovich, B.Y.; Popovichev, V.I.; Ragulskii, V.V.; Faisullov, F.S. Connection between the wavefronts of the reflected and exciting light in stimulated Mandel'shtam Brillouin scattering. In *Landmark Papers on Photorefractive Nonlinear Optics*; World Scientific: London, UK, 1972; Volume 15. Available online: https://en.wikipedia.org/wiki/Brillouin_scattering (accessed on 12 November 2022).

20.    Parker, T.R.; Farhadiroushan, M.; Handerek, V.A.; Rogers, A.J. Temperature and strain dependence of the power level and frequency of spontaneous Brillouin scattering in optical fibers. *Opt. Lett.* **1997**, *22*, 787–789. [CrossRef]

21.    Deligiannakis, G.; Pallikarakis, A.; Papanikolaou, I.; Alexiou, S.; Reicherter, K. Detecting and Monitoring Early Post-Fire Sliding Phenomena Using UAV–SfM Photogrammetry and t-LiDAR-Derived Point Clouds. *Fire* **2021**, *4*, 87. [CrossRef]

22.    Mahalingam, R.; Olsen, M.J.; O'Banion, M.S. Evaluation of landslide susceptibility mapping techniques using lidar-derived conditioning factors (Oregon case study). *Geomat. Nat. Hazards Risk* **2016**, *7*, 1884–1907. [CrossRef]

23.    Watts, C.F.; McClellan, E.A.; Stephenson, G.C. *Implementation of Unmanned Aerial System-Based (UAS) Digital Photogrammetry for Design, Risk Analysis, and Hazard Mitigation of Rock Slopes*; (No. FHWA/VTRC 22-R16, VTRC 22-R16); Virginia Transportation Research Council (VTRC): Charlottesville, VA, USA, 2021.

24.    Mozas-Calvache, A.T.; Pérez-García, J.L.; Fernández-del Castillo, T. Monitoring of landslide displacements using UAS and control methods based on lines. *Landslides* **2017**, *14*, 2115–2128. [CrossRef]

25.    Ford, G. 2021. Available online: https://eas2.unl.edu/~tfrank/History%20on%20the%20Rocks/Teachers/Plan%20files/Ford_GeohistNE.pdf (accessed on 10 October 2021).

26.    Song, C.R.; Bahmyari, H.; Bitar, L.; Amelian, S. *Nebraska Specific Slope Design Manual*; Nebraska Transportation Center, Nebraska Department of Transportation: Lincoln, NE, USA, 2019.

27.    Eversoll, D.A. *Landslides of Nebraska*; Conservation and Survey Division, UNL: Lincoln, NE, USA, 2013; p. 4.

28.    Bekele, B.; Song, C.; Lindemann, M. A Case Study on the Progressive Failure Mechanism of I-180 Slope Using Numerical and Field Observations. *Int. J. Geoengin. Case Hist.* **2021**, *7*, 1–21. [CrossRef]

29.    Song, C.R.; Bitar, L.; Wood, R.L.; Kim, Y.R.; Eun, J.; Bekele, B.; Abualshar, B. *Biopolymerized Slope/Subgrade Stabilizaton and Advanced Field Monitoring*; NTC:26-1121-4052-001; Nebraska Department of Transportation: Lincoln, NE, USA, 2021; 132p.

30.    Chudley, T.R.; Christoffersen, P.; Doyle, S.H.; Abellan, A.; Snooke, N. High-accuracy UAV photogrammetry of ice sheet dynamics with no ground control. *Cryosphere* **2019**, *13*, 955–968. [CrossRef]

31.    Lague, D.; Brodu, N.; Leroux, J. Accurate 3D comparison of complex topography with terrestrial laser scanner: Application to the Rangitikei canyon (NZ). *ISPRS J. Photogramm. Remote Sens.* **2013**, *82*, 10–26. [CrossRef]

32.    DiFrancesco, P.M.; Bonneau, D.; Hutchinson, D.J. The implications of M3C2 projection diameter on 3D semi-automated rockfall extraction from sequential terrestrial laser scanning point clouds. *Remote Sens.* **2020**, *12*, 1885. [CrossRef]

33.    Bolhasan, A.; Wood, R.L.; Abualshar, B.; Wittich, C.E.; Song, C.R.; Guo, J.; Liao, Y. *Data-Driven Prioritization and Empirical Predictions for Bridge Scour in Nebraska (No. M104)*; Nebraska Department of Transportation: Lincoln, NE, USA, 2022.

34.    Song, C.R.; Stokoe, K.H., II. Dynamic Properties of Soils at High Amplitude (with emphasis on threshold strain). *J. Korean Geotech. Soc.* **1991**, *7*, 11–18.

35.    Krietsch, H.; Gischig, V.; Jalali, M.R.; Doetsch, J.; Valley, B.; Amann, F. A comparison of FBG- and Brillouin-strain sensing in the framework of a decameter-scale hydraulic stimulation experiment. In Proceedings of the 52nd U.S. Rock Mechanics/Geomechanics Symposium, Seattle, WA, USA, 17–20 June 2018; ARMA 18-0800.